ELSEVIER

Volume 182, Number 11, November 2009

JOURNAL OF SOLID STATE CHEMISTRY

www.elsevier.com/locate/jssc

CONTENTS

Abstracted/indexed in BioEngineering Abstracts, Chemical Abstracts, Coal Abstracts, Current Contents/Physics, Chemical, & Earth Sciences, Engineering Index, Research Alert, SCISEARCH, Science Abstracts, and Science Citation Index. Also covered in the abstract and citation database SCOPUS®. Full text available on ScienceDirect®.

Regular Articles

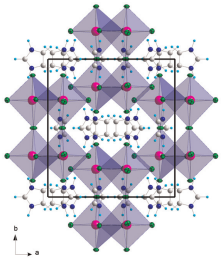

$[C_3N_2H_5]_6[Bi_4Br_{18}]$ has been synthesized and characterized by the X-ray (at 293 and 110 K), calorimetric, dilatometric and dielectric measurements. A crystal structure consists of disordered imidazolium cations and ordered discrete tetramers of $[Bi_4Br_{18}]^{6-}$.

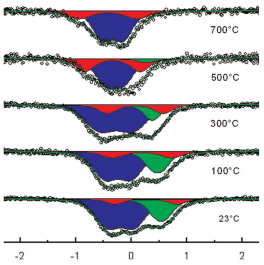

At room temperature, the iron in a high-performance perovskite for ceramic oxygen separation membranes is in a mixed valence state of 75% Fe^{4+} in the high-spin state and 25% Fe^{3+} predominantly in the low-spin state. When heated to 900 °C, a slight reduction of iron is observed that increases the quantity of Fe^{3+} species. However, the dominant occurrence is a gradual transition in the spin-state of trivalent iron from a mixed low-spin/high-spin to a pure high-spin configuration.

Regular Articles—Continued

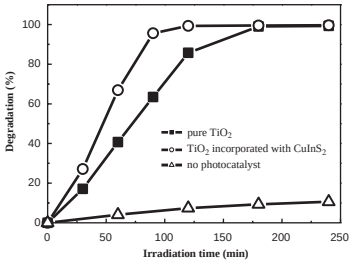

Kinetic curves of 4-nitrophenol (1.44×10^{-4} mol L^{-1}) degradation under UV irradiation.

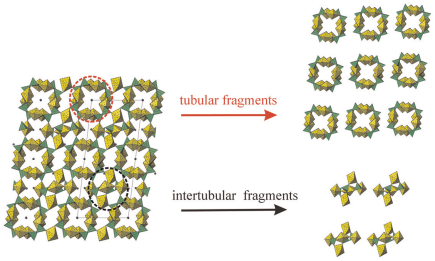

The crystal structures of $Li_5[(UO_2)_{13}(AsO_4)_9(As_2O_7)]$ separated into tubular units and intertubular complexes.

Continued

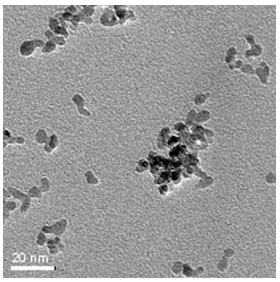

Nanoparticles of YSZ can be synthesized in subcritical and supercritical water using a hydrothermal flow reaction system. Given is the TEM image of YSZ nanoparticles.

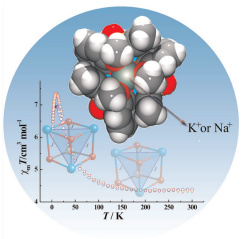

Solvothermal reaction assisted with microwave leads to two heterometallic cubic clusters with 6-metallacrown-3 structure $[Ni_3O_3(OH)]^-$ acting as a host for a K^+ or Na^+ ion. The $\{Ni_3M'O_4\}$ ($M' = K$, Na) cores display dominant ferromagnetic interactions.

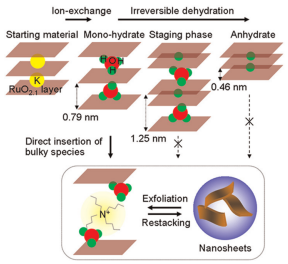

Layered protonic ruthenate derived from a potassium form was directly reacted with bulky tetrabutylammonium ions to trigger exfoliation into nanosheets as long as it is highly hydrated.

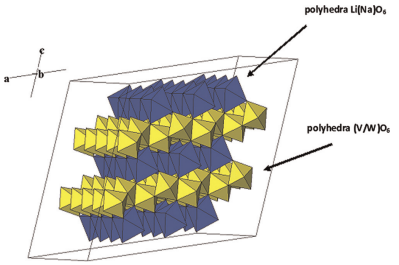

Fragment of the structure of $Li(Na)VWO_6$.

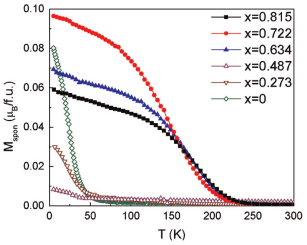

$Lu_{1-x}La_xMn_2O_5$ samples with x up to 0.815 were synthesized and a magnetic phase with an onset transition temperature ~200 K was found in the La-rich compositions.

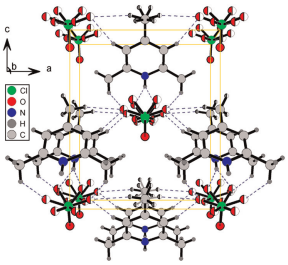

A novel organic–inorganic hybrid material, simple ionic salt: 2,4,6-trimethylpyridinium perchlorate, $[(CH_3)_3C_5H_2NH][ClO_4]$ has been synthesized. In this paper we report singlecrystal X-ray, powder X-ray, calorimetric, dilatometric, dielectric and pyroelectric studies of this compound over a wide temperature range. A possible mechanism of the structural phase transitions in $[(CH_3)_3C_5H_2NH][ClO_4]$ is discussed with particular attention focused on unusually strong pyroelectric properties.

Structural, magnetic, and thermal characteristics of the phase transitions in $Gd_5Ga_xGe_{4-x}$ magnetocaloric materials
Sumohan Misra, Yurij Mozharivskyj, Alexandra O. Tsokol, Deborah L. Schlagel, Thomas A. Lograsso and Gordon J. Miller
Page 3031

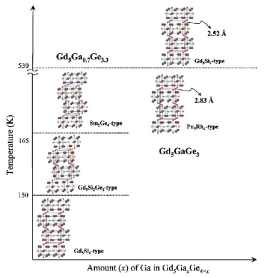

Phase transformations in $Gd_5Ga_xGe_{4-x}$ magnetocaloric materials as a function of temperature.

Pressure-induced coordination changes in $LiBO_2$
Li Lei, Duanwei He, Kai He, Jiaqian Qin and Shanmin Wang
Page 3041

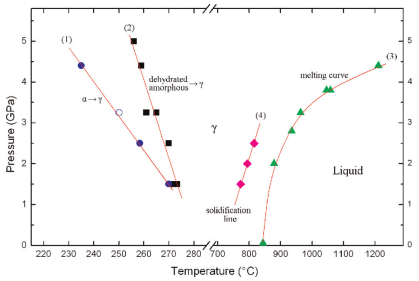

Constructing the pressure–temperature phase diagram for $LiBO_2$.

Formation of helix-containing rods in a hybrid inorganic–organic material
Zhanhui Yuan, William Clegg and Martin P. Attfield
Page 3049

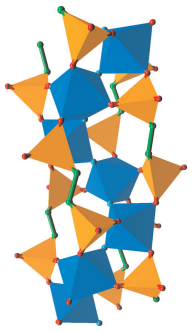

Helical chains of corner-shared *cis*-AlO_4F_2 octahedra form the core of well-separated anionic $[Al_2(O_3PCH_2CH_2PO_3)_2F_2]^{4-}$ rods in the novel hybrid aluminum diphosphonate material, $(H_4tren)[Al_2(O_3PCH_2CH_2PO_3)_2F_2]\bullet(H_2O)$. The incorporation of the organic components into this hybrid material has aided the adoption of a uni-dimensional structure and a specific structural aspect, the helical pitch, within the resulting material, which indicates the potential of this approach to form particular structural features within hybrid materials.

Crystal growth and magnetic behavior of $R_6T_{13-x}Al_xM_y$ phases (R = La, Nd; T = Mn, Fe; M = main group) grown from lanthanide-rich eutectic fluxes
Evan M. Benbow, Naresh S. Dalal and Susan E. Latturner
Page 3055

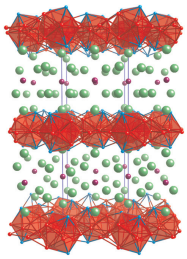

$R_6T_{13-x}Al_xM_y$ phases with the $La_6Co_{11}Ga_3$ structure type crystallize from La/Ni and Nd/Fe eutectics. Transition metal slabs in $La_6Fe_{13-x}Al_xM_y$ and $La_6(Mn/Ni)_{10}Al_3$ order antiferromagnetically (T_N 150 K) and ferromagnetically (T_C 200 K), respectively.

Synthesis, structure characterization and fluorescence property of a new fluoride borate crystal, $CdZn_2KB_2O_6F$
Zhi-Wei Jiao, Fan Zhang, Qing-Feng Yan, De-Zhong Shen and Guang-Qiu Shen
Page 3063

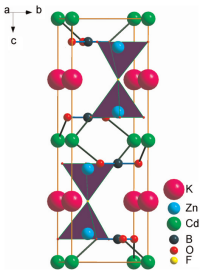

Preparation, structure and fluorescence property of a new fluoride borate crystal, $CdZn_2KB_2O_6F$ are descripted. The crystal represents a new structure type in which $ZnBO_3$ layers are connected through bridging fluorine and cadmium atoms alternately to form a 3D open framework.

A 3D porous indium(III) coordination polymer involving *in-situ* ligand synthesis
Zheng-Bo Han, Yong-Juan Song, Jian-Wei Ji, Wei Zhang and Guang-Xi Han
Page 3067

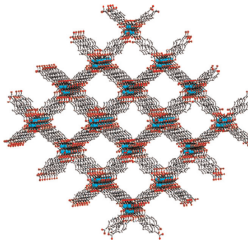

The hydrothermal reaction of In^{3+} and 1,2,4-benzenetricarboxylic acid with the presence of piperazine leads to the generation of a novel 3D porous coordination polymer, $[H_3O][In_2(btc)(bdc)(OH)_2]\cdot 5.5H_2O$, (btc = 1,2,4-benzenetricarboxylate, bdc = 1,4-benzenedicarboxylate).

Continued

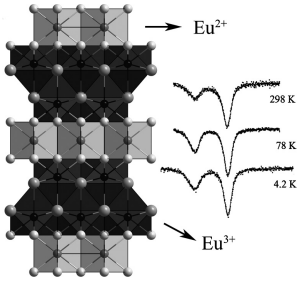

Crystal structure and ^{151}Eu-Mössbauer spectra of mixed-valent $Eu_3F_4S_2$.

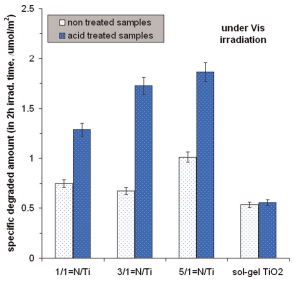

The effect of the acid treatment on the visible-light-driven photocatalytic activity of the N-doped, anatase TiO_2 catalysts.

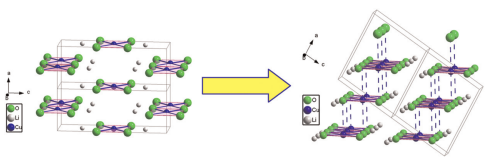

Li_2CuO_2 undergoes a first-order transition from the ambient orthorhombic to a monoclinic phase at above 5.4 GPa with coordination change from four-square to six-octahedron.

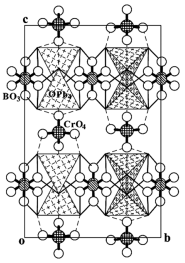

$(Pb_3O)_2(BO_3)_2MO_4$ (M = Cr, Mo) are characterized by 1D $^1_\infty[Pb_3O]^{4+}$ chains formed by corner-sharing OPb_4 tetrahedra. BO_3 and CrO_4 (MoO_4) groups are located around the chains to hold them together via Pb–O bonds.

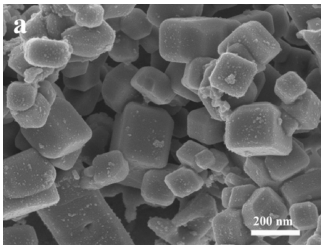

FESEM images of CeB_6 nanocubes prepared at 500 °C for 12 h using B_2O_3 as boron resource.

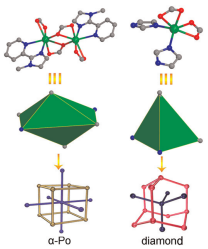

A series of three-dimensional interpenetrating metal-organic frameworks based on different polygons or polyhedra has been synthesized. The crystal structures and topological analysis of these compounds, along with a systematic investigation of the relationship between topological types and molecular building blocks, will be discussed.

A new material for hydrogen storage; $ScAl_{0.8}Mg_{0.2}$
Martin Sahlberg, Premysl Beran, Thomas Kollin Nielsen, Yngve Cerenius, Krisztina Kadás, Marko P.J. Punkkinen, Levente Vitos, Olle Eriksson, Torben R. Jensen and Yvonne Andersson
Page 3113

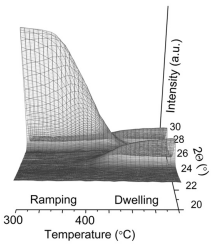

Hydrogen absorption in $ScAl_{0.8}Mg_{0.2}$ studied by *in situ* synchrotron radiation powder X-ray diffraction. The hydrogen absorption properties were studied by neutron diffraction and quantum mechanical calculations.

Preparation, crystal structure and luminescent properties of the (6,3) type network supramolecular lanthanide picrate complexes with 2,2′-[(1,2-naphthalene)bis(oxy)]bis [N-(phenylmethyl)]acetamide
Qin Wang, Kuan-Zhen Tang, Wei-Sheng Liu, Yu Tang and Min-Yu Tan
Page 3118

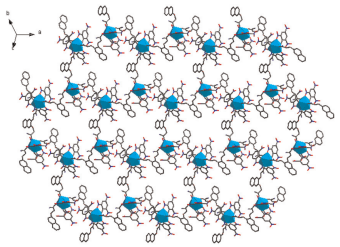

The (6,3) type network supramolecular luminescent lanthanide picrate complexes $\{Ln_2L_3(Pic)_6\}_n$ (L = 2,2′-[(1,2-naphthalene)bis(oxy)] bis[N-(phenylmethyl)]acetamide) displaying a two-dimensional honeycomb-like framework have been designed and prepared.

Novel building units with bimetallic rings in inorganic/organic hybrid chains and layers
Thushitha Mahenthirarajah, Yang Li and Philip Lightfoot
Page 3125

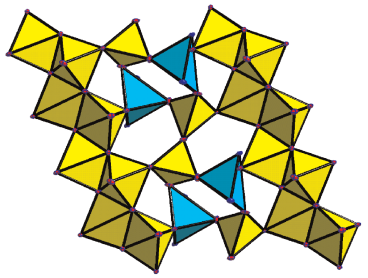

Hydrothermal synthesis is used to prepare hybrid mixed metal oxides and oxyfluorides with novel extended connectivities.

$Ba_5Ti_{12}Sb_{19+x}$, a polar intermetallic compound with a stuffed γ-brass structure
Haiying Bie and Arthur Mar
Page 3131

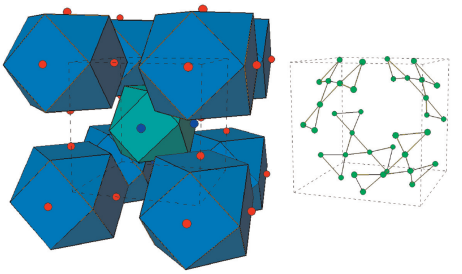

A γ-brass substructure built up of Ba–Sb clusters is stuffed with planar Ti_9 clusters.

Fabrication and thermoelectric properties of fine-grained TiNiSn compounds
Minmin Zou, Jing-Feng Li, Bing Du, Dawei Liu and Takuji Kita
Page 3138

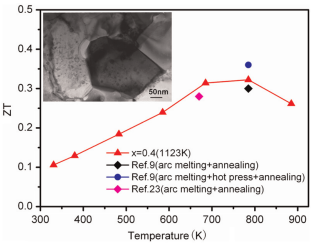

Nearly single-phased TiNiSn-based half-Heusler compound polycrystalline materials with fine grains were fabricated by combining mechanical alloying (MA) and spark plasma sintering (SPS). A high ZT value for undoped TiNiSn was obtained because of the reduced thermal conductivity.

Flux synthesis of (3,4)-connected zinc phosphites with different framework topologies
Zhien Lin and Stefanie Dehnen
Page 3143

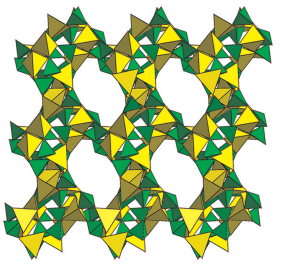

Two three-dimensional open-framework zinc phosphites have been synthesized by a phosphorous acid flux method. The two compounds are constructed from $Zn_3(HPO_3)_4$ clusters and have noz and pcu topologies, respectively.

Continued

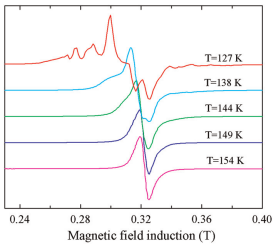

Temperature dependent evolution of the ESR spectrum for the $(Cd_{0.56}Sb_{0.44})[Cr_2]Se_4$ single-crystal showing inhomogeneous nature of the ferromagnetic ordered state below $T_c = 130$ K. At temperature 127 K a fraction of the paramagnetic phase can still be observed.

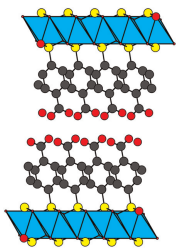

Three new copper carboxyphenylphosphonates were synthesized. Layered structure of one of them, $CuH(OOCC_6H_4PO_3)$, is composed of CuO_6 octahedra arranged hexagonally around two phosphonate groups, which have their carboxyphenyl groups extending into the space above and below the copper–phosphonate layer.

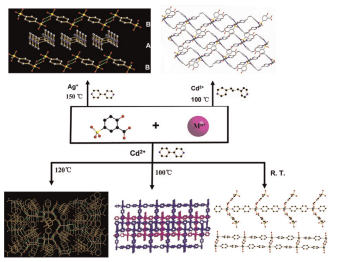

Reactions of 5-sulfosalicylic acid (H_3L) and d^{10} metal ions (Cd^{II}, Ag^{I}) produce five new complexes. Complexes **1–4** all display green luminescences at room temperature.

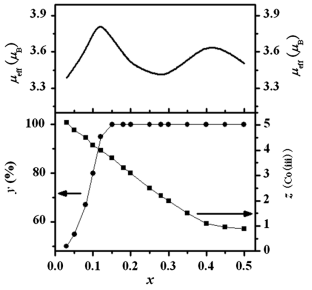

x dependence of the calculated results from a phase separation model.

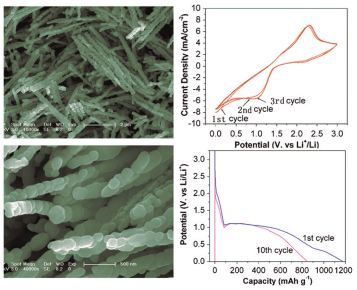

The porous Co_3O_4 nanorods synthesized via a microemulsion-based method in combination with subsequent calcination were applied in the negative electrode materials for lithium-ion batteries and exhibited high electrochemical performance.

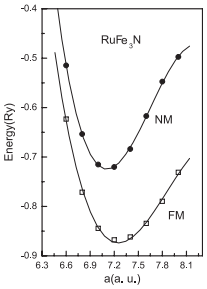

Total energy curves, versus lattice spacing for the $RuFe_3N$ nitride. It is observed an energy difference between ferromagnetic and paramagnetic states, which provides high critic pressure.

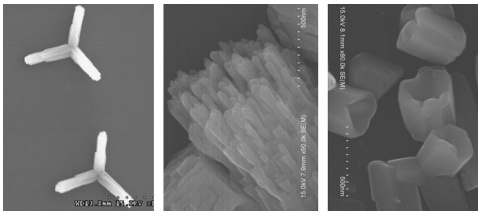

A facile and effective carbon-assisted thermal evaporation method is explored to synthesize CdS multipods, nanobrushes and nanocups. These CdS nanostructures display very different optical properties.

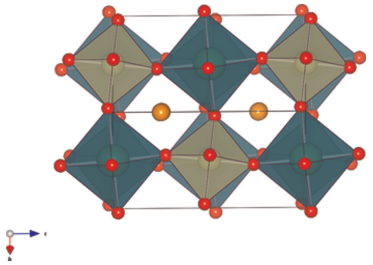

Variable temperature neutron and synchrotron X-ray powder diffraction methods have been used to resolve the long standing question regarding the symmetry and structure of the cation-ordered perovskite Ba_2LaIrO_6. We show this is monoclinic in $I2/m$ at room temperature, with the sequence of phases $I\bar{1}$ $I2/m$ $R\bar{3}$ $Fm\bar{3}m$.

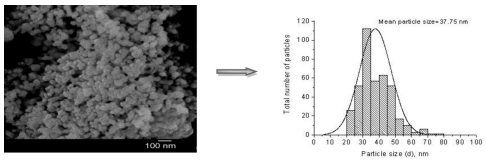

Silicon nanoparticles 37.75 nm in mean diameter was obtained by rapid metathesis reaction performed in $Na_2SiF_6 + 4NaN_3$ powder bed diluted with NaF.

Rapid Communications

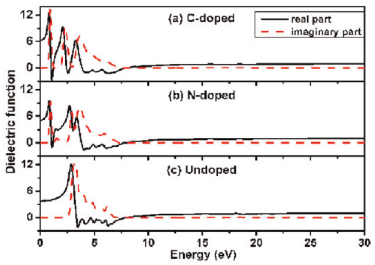

By first-principles calculations, it is predicted that substitutional doping of C (or N) in c-CeO_2 lowers E_g and also O 2p–Ce 4f gap, and increases O 2p–Ce 4f transition intensity.

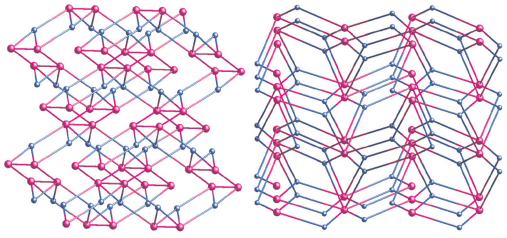

This work presents a series of 3-D metal-organic frameworks with 3-pyridin-4-yl-benzoate, which display new (3,6)-connected net topologies of $(3.4.5)(3^2.4^4.5^5.6^2.7^2)$ for $Mn^{II}/Zn^{II}/Cd^{II}$ and $(4^2.6)_2(4^4.6^2.8^9)$ for Pb^{II} species.

Corrigendum

Continued

Author inquiries

For inquiries relating to the submission of articles (including electronic submission where available) please visit this journal's homepage at http://www.elsevier.com/locate/jssc. You can track accepted articles at http://www.elsevier.com/trackarticle and set up e-mail alerts to inform you of when an article's status has changed. Also accessible from here is information on copyright, frequently asked questions and more.
Contact details for questions arising after acceptance of an article, especially those relating to proofs, will be provided by the publisher.

Language services. Authors who require information about language editing and copyediting services pre- and post-submission please visit http://www.elsevier.com/locate/languagepolishing or our customer support site at http://epsupport.elsevier.com. Please note Elsevier neither endorses nor takes responsibility for any products, goods or services offered by outside vendors through our services or in any advertising. For more information please refer to our Terms & Conditions http://www.elsevier.com/termsandconditions

For a full and complete Guide for Authors, please go to: http://www.elsevier.com/locate/jssc

Journal of Solid State Chemistry has no page charges.